Editors' Suggestion

Quick charging of a quantum battery with superposed trajectories

Po-Rong Lai,[1,*] Jhen-Dong Lin,[1,*] Yi-Te Huang,[1] Hsien-Chao Jan,[1] and Yueh-Nan Chen[1,2,†]
[1]*Department of Physics and Center for Quantum Frontiers of Research & Technology (QFort), National Cheng Kung University, Tainan 701, Taiwan*
[2]*Physics Division, National Center for Theoretical Sciences, Taipei 10617, Taiwan*

(Received 28 July 2023; accepted 29 March 2024; published 7 May 2024)

We propose charging protocols for quantum batteries based on quantum superpositions of trajectories. Specifically, we consider that a qubit (the battery) interacts with multiple cavities or a single cavity at various positions, where the cavities act as chargers. Further, we introduce a quantum control prepared in a quantum superposition state, allowing the battery to be simultaneously charged by multiple cavities (the multiple-charger protocol) or a single cavity with different entry positions (the single-charger protocol). To assess the battery's performance, we evaluate the maximum extractable work, referred to as ergotropy. The primary discovery lies in the quick charging effect, wherein we prove that the increase in ergotropy stems from the quantum coherence initially present in the quantum control. Moreover, the induced "Dicke-type interference effect" in the single-charger protocol can further lead to a "perfect charging phenomenon", enabling a complete conversion of the stored energy into extractable work across the entire charging process, with just two entry positions in superposition. Furthermore, we propose circuit models for these charging protocols and conduct proof-of-principle demonstrations on IBMQ and IonQ quantum processors. The results validate our theoretical predictions, demonstrating a clear enhancement in ergotropy.

DOI: 10.1103/PhysRevResearch.6.023136

I. INTRODUCTION

Quantum batteries (QBs) have emerged as a popular research topic, providing valuable insights into how thermodynamics functions at the quantum scale [1–4]. Recent development has demonstrated that various quantum resources such as entanglement [5,6] or coherence [7,8] can enhance the performance of quantum batteries in terms of charging [9–19], storage [20–26], and work extraction [27–37], etc. One of the intriguing phenomena used to achieve these enhancements is the collective effects triggered by a group of QBs [10,11,21,38–42]. In his seminal paper [43], Dicke characterized one of the collective effects, superradiance, by the quantum interference of emissions from an ensemble of atoms. Recent investigations have also demonstrated the utility of the time-reversed phenomenon, known as superabsorption [39,40,44,45], on enhancing the capabilities of QBs.

In this work, our focus lies on an interferometric approach known as "superpositions of trajectories" [46–57]. This approach utilizes a Mach-Zehnder interferometer (MZI) and treats an atom's space-time trajectories as a quantum system, enabling the exploration of quantum interference of these trajectories. A notable outcome of this approach is the effective noise mitigation in various quantum information tasks [50,51,53,56,57]. In our recent work [54], we have further advanced the understanding by interpreting this noise mitigation as a Zeno-type state freezing phenomenon [58] within the framework of open quantum systems [59]. Additionally, we have demonstrated that this approach can also manifest Dicke-type interference effects even when only one single atom is involved. Building upon these insights, this work aims to delve into the potential of leveraging superpositions of trajectories to enhance the performance of QBs.

We consider a qubit acting as the quantum battery, gaining energy through interactions with cavities functioning as chargers. To assess the QB's performance, we focus on the maximum extractable work, known as ergotropy [27]. The ergotropy is bounded by the stored energy, i.e., the change in the qubit's internal energy, which can be regarded as a consequence of energy conservation. To utilize superposed trajectories, we propose two charging protocols using an MZI setup akin to scenarios in Ref. [54]. The first one is called the multiple-charger protocol, which consists of multiple identical chargers (cavities), and the QB can interact with these chargers in a manner of quantum superposition via a multiport beam splitter. In principle, there are multiple output beams of QB when it exits the interferometer. This enables us to adjust the work extraction strategy for each output and obtain an average ergotropy, also known as the daemonic ergotropy [28,60]. The primary result of this protocol is an "activation" of the ergotropy. Specifically, we demonstrate

*These authors contributed equally to this work.
†yuehnan@mail.ncku.edu.tw

that when the battery is charged by a single cavity (without utilizing superposed trajectories), the ergotropy remains zero for a certain period, despite storing energy immediately after interaction with the cavity. Thus, there exists a finite delay before the battery can store "useful energy", i.e., extractable work. According to the definition of ergotropy, population inversion, i.e., the excited state population of the qubit being larger than its ground state population, is required to obtain a nontrivial ergotropy. Therefore, one must wait until the battery reaches the inversion point to obtain extractable work.

Remarkably, we demonstrate that by considering this multiple-charger protocol, nonzero ergotropy can be obtained right after the charging process begins. This implies that this protocol enables the achievement of "quick charging" for the QB, where the ergotropy can be activated before reaching the inversion point. We observe that the ergotropy increases as the number of superposed trajectories grows. In the limit of an infinite number of superposed trajectories and considering the strong-coupling regime (where the rotating-wave approximation is valid), we observe a "perfect charging result" with a complete conversion of stored energy into extractable work throughout the entire charging process. To gain a deeper insight, we prove that the initial coherence of the quantum control is the necessary resource for ergotropy enhancement. Furthermore, we reveal that the degree of the ergotropy enhancement is proportional to the initial coherence.

The second protocol is coined the single-charger protocol with only one cavity (charger) involved. In this protocol, the QB can enter from different positions into the cavity, experiencing different coupling strengths with the cavity. By using the superposed trajectories, the QB can enter these various positions simultaneously. As indicated in Ref. [54], this particular setup can induce the Dicke-type interference effect. Notably, we show that two entry positions in quantum superposition are sufficient to trigger the "perfect charging result" regardless of the coupling strength. Furthermore, we investigate the potential work costs for introducing the quantum control and the impact of scaling up the number of qubit batteries. The results suggest that the single-charger protocol, harnessing the underlying Dicke-type interference effect, emerges as a more advantageous design, offering benefits in terms of both resource consumption and overall performance.

Additionally, we present quantum circuits designed for the aforementioned charging protocols, requiring fewer than 20 two-qubit gates. We implement and execute these circuits on both IonQ quantum processors (based on trapped ions) and IBMQ quantum processors (based on superconducting circuits). The experimental results obtained from these implementations further validate the increase in ergotropy, which is consistent with our theoretical predictions.

The rest of the paper is organized as follows. In Sec. II, we characterize the multiple-charger protocol. In Sec. III, we further investigate the single-charger protocol. In Sec. IV, we investigate the potential work cost for introducing the quantum control. In Sec. V, we explore the impact of scaling up the number of batteries for both protocols. In Sec. VI, we consider the circuit implementations and present the experimental results of the devices from IBMQ and IonQ. Finally, we draw our conclusions in Sec. VII.

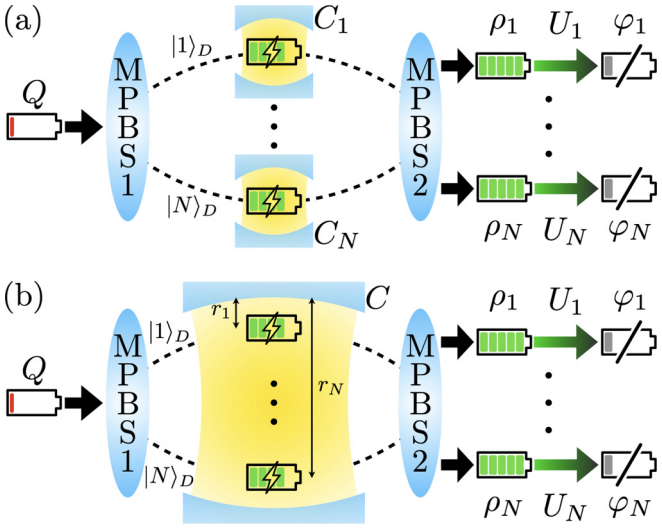

FIG. 1. The quantum battery Q is first sent into a multiport beam splitter (MPBS1), which allows the quantum battery to travel along N different trajectories (denoted by $|j\rangle_D$ with $j = 1 \ldots N$) in a manner of quantum superposition. We consider two charging processes: (a) the trajectories each lead to a charger (cavities) $\{C_j\}$, causing the quantum battery to interact with all chargers simultaneously, (b) the trajectories lead to a single charger C but at different positions $\{r_j\}$, causing the quantum battery to interact with the charger with various coupling strengths. Once the charging process is completed, a second multiport beam splitter (MPBS2) is used to perform measurement on the trajectories' degree of freedom D. This measurement captures the quantum interference effect between different trajectories and results in N possible reduced states ρ_j. We then extract work from each ρ_j, where the maximum amount of extractable work is called the ergotropy. The work extraction operations are described by unitary operators U_j, which transform each of the batteries to a passive state φ_j.

II. MULTIPLE-CHARGER PROTOCOL: QUICK CHARGING THROUGH QUANTUM COHERENCE

In this section, we formulate the multiple-charger scenario, which can be described by a MZI as shown in Fig. 1(a). The MZI is constructed by two multiport beam splitters, MPBS1 and MPBS2. The first beam splitter (MPBS1) bifurcates the battery's trajectories, while the second one (MPBS2) enables the quantum interference between these trajectories. In the following, we demonstrate the quick charging effect through the interferometric setup. Further, we prove that the ergotropy enhancement originates from the quantum coherence of the superposed trajectories.

Let us now delve into the detailed description of the charging protocol, which consists of three different components: (i) A qubit Q, which acts as the quantum battery. (ii) N identical single-mode cavities $\{C_j\}_{j=1\ldots N}$, which act as the chargers. The QB moves at a speed v and gets charged when it passes through one of the chargers. Suppose that the cavity length is l. Then, the interaction time reads as $\tau = l/v$. To simplify our discussions, we assume that the cavity is homogeneous such that the interaction strength between the QB and the charger remains constant during the charging process [61]. (iii) We characterize the trajectory degrees of

freedom as an N-dimensional qudit D, wherein we associate N different trajectories inside the interferometer with N basis states $\{|j\rangle_D\}_{j=1\ldots N}$. When the QB takes the path labeled by j, it interacts with the charger C_j. In other words, D acts as a quantum control that determines which charger the QB interacts with. The total Hamiltonian involving these three components can then be written as

$$H_{\text{tot}} = \sum_{j=1}^{N} |j\rangle\langle j|_D \otimes H_{QC_j}. \tag{1}$$

The Hamiltonian H_{QC_j} of the quantum battery Q and the charger C_j can be expressed as

$$\begin{aligned} H_{QC_j} &= H_Q + H_{C_j} + H'_{QC_j}, \\ H_Q &= \frac{\hbar}{2}\omega_a\hat{\sigma}_z = \frac{\hbar}{2}\omega_c\hat{\sigma}_z, \\ H_{C_j} &= \hbar\omega_c\hat{a}_j^\dagger\hat{a}_j, \\ H'_{QC_j} &= \hbar\omega_c\lambda\hat{\sigma}_x(\hat{a}_j + \hat{a}_j^\dagger). \end{aligned} \tag{2}$$

Here, $\hat{a}_j(\hat{a}_j^\dagger)$ annihilates (creates) a photon in C_j with frequency ω_c, $\hbar\omega_a$ represents the energy splitting between the ground state $|g\rangle$ and the excited state $|e\rangle$ of Q. The Pauli operators are therefore given by $\hat{\sigma}_z = |e\rangle\langle e| - |g\rangle\langle g|$ and $\hat{\sigma}_x = |e\rangle\langle g| + |g\rangle\langle e|$. Moreover, the dimensionless constant λ represents the coupling strength between Q and all the chargers. Throughout this work, we focus on the resonant regime $\omega_a = \omega_c$.

We first send the battery Q into the multiport beam splitter (MPBS1 in Fig. 1). In general, the beam splitter can prepare the trajectories in a quantum superposition state so that Q can be charged by these N chargers simultaneously. For simplicity, we assume the superposition state of the trajectories is

$$|\psi\rangle_D = \frac{1}{\sqrt{N}}\sum_{j=1}^{N}|j\rangle_D\,. \tag{3}$$

We consider that the battery and chargers are initialized in the ground state and the single-photon Fock state, respectively. Therefore, the total initial state reads as

$$|\psi(0)\rangle_{DQC} = \frac{1}{\sqrt{N}}\sum_{j=1}^{N}|j\rangle_D \otimes |g\rangle_Q \bigotimes_{j'=1}^{N}|1\rangle_{C_{j'}}\,. \tag{4}$$

After Q interacts with the chargers, according to Eq. (1), the total states becomes

$$|\psi(\tau)\rangle_{DQC} = \frac{1}{\sqrt{N}}\sum_{j=1}^{N}|j\rangle_D \otimes |\phi_j(\tau)\rangle_{QC}\,, \tag{5}$$

where $|\phi_j(\tau)\rangle_{QC}$ is defined as

$$|\phi_j(\tau)\rangle_{QC} = \exp\left(-i\frac{\tau}{\hbar}H_{QC_j}\right)\left(|g\rangle_Q \bigotimes_{j'=1}^{N}|1\rangle_{C_{j'}}\right). \tag{6}$$

Finally, we make these trajectories interfere with one another by using another beam splitter (MPBS2 in Fig. 1). In principle, MPBS2 has N different outputs, which can be described using a set of orthonormal projectors $\{P_k\}_k$ acting on D, namely,

$$\begin{aligned} &P_k = |\xi_k\rangle\langle\xi_k|_D\,, \\ &\sum_{k=1}^{N} P_k = \mathbb{1}, \\ &\langle\xi_k|\xi_{k'}\rangle = \delta_{k,k'}\ \forall\ k, k'. \end{aligned} \tag{7}$$

Therefore, the (unnormalized) reduced state for the system Q with the output k reads as

$$\sigma_k(\tau) = \text{Tr}_{CD}[P_k\,|\psi(\tau)\rangle\langle\psi(\tau)|_{DQC}\,P_k]. \tag{8}$$

Note that the probability of obtaining the outcome k is $p_k(\tau) = \text{Tr}[\sigma_k(\tau)]$. Thus, the normalized state conditioned on the outcome k can be written as $\rho_k(\tau) = \sigma_k(\tau)/p_k$.

Throughout this work, we choose

$$|\xi_{k=1}\rangle\langle\xi_{k=1}|_D \equiv \frac{1}{N}\sum_{m,n=1}^{N}|m\rangle\langle n|_D\,. \tag{9}$$

According to the assumption that all chargers are identical as well as the orthonormality of the projectors, in Appendix A, we show that the explicit form of the rest of the projectors is irrelevant, enabling us to further simplify the analysis.

Here, we evaluate the performance of a QB by considering the ergotropy, which quantifies the maximum extractable work. Given a charged state of the QB $\rho(\tau)$, the ergotropy is defined as

$$\begin{aligned} W[\rho(\tau)] &\equiv \text{Tr}[\rho(\tau)H_Q] - \min_U \text{Tr}[U\rho(\tau)U^\dagger H_Q] \\ &= \text{Tr}[\rho(\tau)H_Q] - \text{Tr}[\varphi(\tau)H_Q], \end{aligned} \tag{10}$$

where U represents the unitary operation for work extraction. Also, φ is known as the passive state [27] (associated with ρ), which cannot provide useful work for all possible work extraction operations U. According to Ref. [27], the passive state of the battery can be written as

$$\varphi = s_0\,|e\rangle\langle e| + s_1\,|g\rangle\langle g|\,. \tag{11}$$

Here, s_0 and s_1 denote the eigenvalues of ρ with $s_0 < s_1$. Note that the upper limit of the ergotropy is set by the stored energy quantified by the difference in the internal energy of the QB before and after charging, namely,

$$\begin{aligned} E(\tau) &\equiv \sum_{k=1}^{N} p_k(\tau)\text{Tr}[H_Q\rho_k(\tau)] - \text{Tr}(H_Q\,|g\rangle\langle g|) \\ &= \text{Tr}[H_Q\rho(\tau)] - \text{Tr}(H_Q\,|g\rangle\langle g|), \end{aligned} \tag{12}$$

where $\rho(\tau) = \sum_k \sigma_k(\tau)$. We can obtain $W \leqslant E$ because $\text{Tr}(H_Q\,|g\rangle\langle g|) \leqslant \text{Tr}(H_Q\varphi)$ in general. The inequality saturates if and only if $\varphi = |g\rangle\langle g|$, which implies that ρ is a pure state. Further, by employing the Bloch representation of the qubit state, one can find that the extractable work increases as the purity of the qubit also increases (see Appendix B for the detailed derivations).

As aforementioned, in our charging protocol, there are N different outputs (labeled as $\{k\}$). In principle, one can find the optimal work extraction strategies for each output and obtain

the average ergotropy, i.e.,

$$\overline{W} = \sum_k p_k W[\rho_k(\tau)] = \sum_k p_k \{\mathrm{Tr}[\rho_k(\tau)H_Q] - \mathrm{Tr}[\varphi_k(\tau)H_Q]\}, \quad (13)$$

where φ_k denotes the passive state associated with ρ_k. Following similar reasoning as mentioned earlier, the average ergotropy is also upper bonded by the stored energy, and the optimal extractable work can be obtained, i.e., $\overline{W}(\tau) = E(\tau)$, if and only if $\{p_k, \rho_k\}$ forms a pure state decomposition of ρ. In addition, the average extractable work increases as the average purity for the ensemble $\{p_k, \rho_k\}$ increases (see Appendix B for the detailed derivations).

Let us begin with the strong coupling regime [62] (i.e., $\lambda \leqslant 0.1$), where the rotating-wave approximation can be employed. In this case, the interaction Hamiltonian of the QB and the chargers in Eq. (2) can be reduced to the Jaynes-Cummings model, namely,

$$\tilde{H}'_{QC_j} = \hbar\omega_c\lambda(\hat{\sigma}_+\hat{a}_j + \hat{\sigma}_-\hat{a}_j^\dagger), \quad (14)$$

where $\hat{\sigma}_+ = |e\rangle\langle g|$ and $\hat{\sigma}_- = |g\rangle\langle e|$ represent the creation and annihilation operators of Q, respectively. We can then evaluate Eq. (6) in this case:

$$|\phi_j(\tau)\rangle_{QC} = -i\,\sin(\omega_c\lambda\tau)\,|e\rangle_Q \otimes \hat{a}_j \bigotimes_{j'=1}^{N} |1\rangle_{C_{j'}} + \cos(\omega_c\lambda\tau)\,|g\rangle_Q \bigotimes_{j'=1}^{N} |1\rangle_{C_{j'}}. \quad (15)$$

Let us start from the simplest case with only one charger (i.e., $N = 1$), where the reduced state of Q is expressed as

$$\rho(\tau) = \sin^2(\omega_c\lambda\tau)\,|e\rangle\langle e| + \cos^2(\omega_c\lambda\tau)\,|g\rangle\langle g|. \quad (16)$$

In this case, the stored energy is

$$E(\tau) = \hbar\omega_c \sin^2(\omega_c\lambda\tau), \quad (17)$$

which oscillates with a period $T = 2\pi/(\omega_c\lambda)$. We now focus on the time interval $\tau \in [0, T/4]$ (such that $\omega_c\lambda\tau \in [0, \pi/2]$), where the stored energy monotonically increases from 0 to its maximum value $\hbar\omega_c$. Note that ρ is diagonalized under basis $\{|e\rangle, |g\rangle\}$. Thus, according to Eq. (10), the criterion for obtaining nonzero ergotropy is the moment that population inversion occurs, where the excited-state population becomes larger than the ground-state population ($\langle e|\rho(\tau)|e\rangle > \langle g|\rho(\tau)|g\rangle$). The time dependence of the ergotropy can then be derived as

$$W(\tau) = \begin{cases} 0 & \text{if} \quad 0 \leqslant \tau < \frac{T}{8}, \\ \hbar\omega_c[2\,\sin^2(\omega_c\lambda\tau) - 1] & \text{if} \quad \frac{T}{8} \leqslant \tau \leqslant \frac{T}{4}. \end{cases} \quad (18)$$

One can observe that in the duration $\tau \in [0, T/8]$, although the stored energy E monotonically increases, there is no extractable work, $W = 0$, for the battery because ρ remains a passive state during this period.

We now consider the scenario involving N chargers. When the selective measurements satisfy Eqs. (7) and (9), the unnormalized postmeasurement states can be written as (see Appendix A for detailed derivations)

$$\sigma_{k=1}(\tau) = \frac{1}{N}\sin^2(\omega_c\lambda\tau)\,|e\rangle\langle e| + \cos^2(\omega_c\lambda\tau)\,|g\rangle\langle g|,$$
$$\sigma_{k\neq 1}(\tau) = \frac{1}{N}\sin^2(\omega_c\lambda\tau)\,|e\rangle\langle e|. \quad (19)$$

Here, for the case $k = 1$, the postmeasurement state is passive during the time period $\tau \in [0, T_N]$ with the inversion time $T_N = \tan^{-1}(\sqrt{N})T/2\pi$. Remarkably, for the cases of $k \neq 1$, the postmeasurement states are exactly the excited state, implying that the maximal extractable work $\hbar\omega_c$ can be obtained. Therefore, the average ergotropy can be expressed as

$$\overline{W}(\tau) = W[\sigma_{k=1}(\tau)] + (N-1)W[\sigma_{k\neq 1}(\tau)] = \begin{cases} \hbar\omega_c\frac{N-1}{N}\sin^2(\omega_c\lambda\tau) & \text{if} \quad 0 \leqslant \tau \leqslant T_N, \\ \hbar\omega_c[2\,\sin^2(\omega_c\lambda\tau) - 1] & \text{if} \quad T_N \leqslant \tau \leqslant \frac{T}{4}. \end{cases} \quad (20)$$

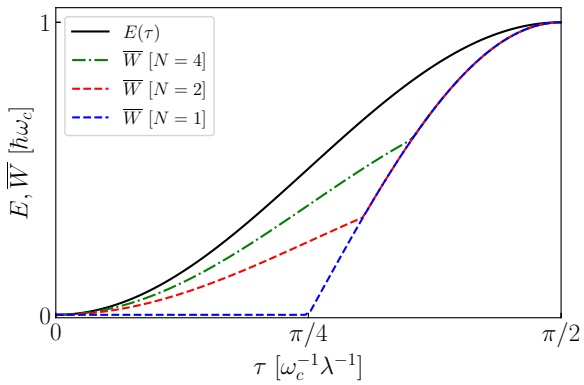

FIG. 2. The stored energy E and average ergotropy $\overline{W}$ (both in units of $\hbar\omega_c$) on time τ (in units of $1/\omega_c$) for $\lambda = 0.05$. The black solid curve plots the stored energy while the dashed curves plot the average ergotropy. From bottom to top, the blue, red, and green dashed curves show the results for $N = 1$, 2, and 4, respectively.

In Fig. 2, we present the time-dependent stored energy and the average ergotropy for different values of N. In contrast to the case of $N = 1$, we observe nonzero average ergotropy for the entire interval of interest because the states with $k \neq 1$ are nonpassive right after the QB-chargers interaction is turned on ($\tau > 0$). Therefore, *the protocol can be used for "quick charging", enabling immediate storage of useful work after the charging process begins*. Furthermore, the result indicates that increasing N delays the inversion time T_N and enhances the average ergotropy before T_N. To gain a deeper understanding, we present the following proposition.

Proposition. The initial coherence of the control qudit serves as a necessary resource for the ergotropy enhancement. In addition, the degree of the enhancement is linearly proportional to the coherence for our scenario. We provide the detailed proof and derivations in Appendix C. In essence, we demonstrate that the lack of initial coherence leads to the control-battery state remaining uncorrelated throughout the entire charging process, thereby resulting in no enhancement in the ergotropy. Further, when all the off-diagonal terms of the control qudit are identical, the degree of the enhancement is directly proportional to the amount of the initial coherence. Consequently, it can be inferred that the

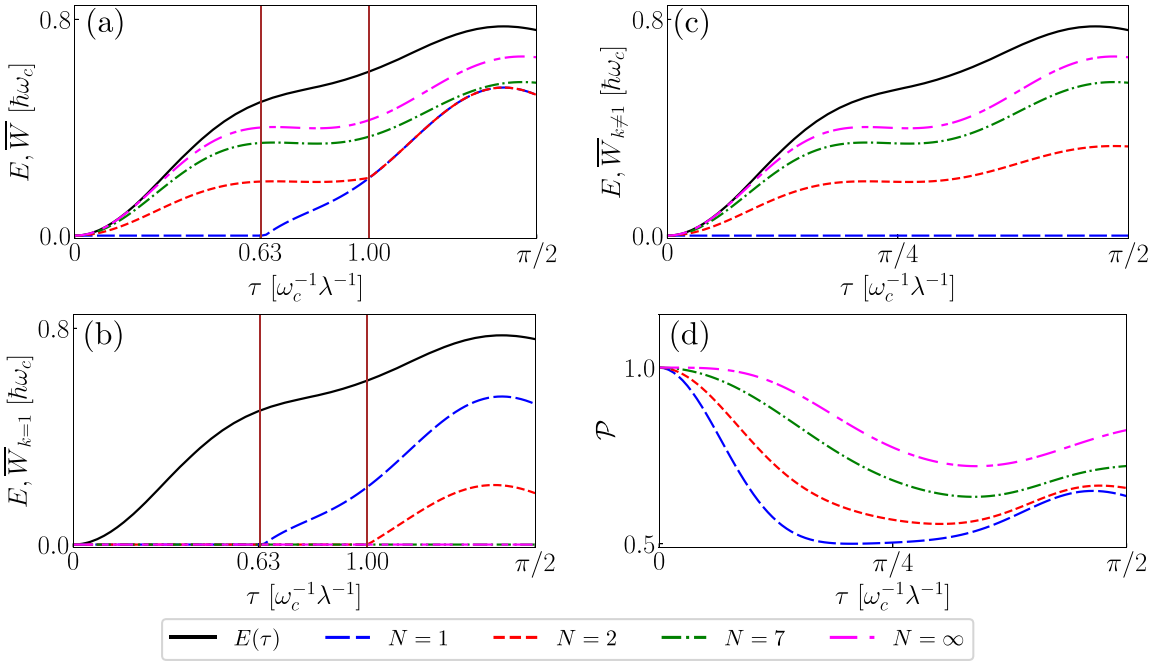

FIG. 3. (a) The stored energy E and average ergotropy $\overline{W}$ (both in units of $\hbar\omega_c$) as functions of time τ (in units of $1/\omega_c$) for $\lambda = 0.5$. (b) The stored energy E and the average ergotropy contributed by states of $k = 1$, $\overline{W}_{k=1}$. Two brown vertical lines at $\tau = 0.63, 1.00$ indicate the inversion points T_N for $N = 1$ (blue) and $N = 2$ (red). Here, $\overline{W}_{k=1}$ is 0 when $N = 7$ (green) and $N = \infty$ (magenta). (c) The stored energy E and the average ergotropy contributed by states of $k \neq 1$, $\overline{W}_{k\neq1}$. Except for $N = 1$ (blue), these states contribute average ergotropy when $\tau > 0$. (d) The dashed curves plot the change in average purity $\mathcal{P}$ against time τ. The cutoff photon number is set to 9 in the above results.

quick charging effect stems from the initial coherence of the quantum control. Furthermore, from the perspective of qubit-only dynamics presented in Eq. (19), the enhancement can be further linked to the Zeno-type state freezing effect [54], for the postmeasurement state with $k = 1$. Specifically, as the number of superposed trajectories N increases, the excited-state population of the postmeasurement state $\sigma_{k=1}$ decreases, indicating its convergence towards the ground state. Consequently, the qubit dynamics associated with this specific outcome decelerates. In the asymptotic limit ($N \to \infty$), the population of the excited state for this outcome diminishes to zero, resulting in the qubit frozen in the ground state. Notably, as the postmeasurement state with $k = 1$ approaches the ground state, its purity also increases. Additionally, as inferred from Eq. (19), the postmeasurement state with $k \neq 1$ stays in the (pure) excited state throughout the entire charging process. Thus, the Zeno-type effect contributes to an overall increase in the average purity, consequently enhancing the ergotropy as previously mentioned. Finally, with infinite superposed trajectories, the postmeasurement states are pure (namely, $\sigma_{k=1}(\tau) \propto |g\rangle\langle g|$ and $\sigma_{k\neq1}(\tau) \propto |e\rangle\langle e|$). This signifies a "perfect charging result", where the stored energy can be completely converted into extractable work over the entire time interval, i.e., $E(\tau) = \overline{W}(\tau)$.

We now extend our scope of discussion into the ultrastrong coupling regime [62], where the rotating-wave approximation is no longer valid. In Fig. 3(a), we present the dynamics of the average ergotropy and the stored energy. We can still observe the quick charging effect, a delay of the inversion point, and an enhancement in average ergotropy as N increases. As shown in Figs. 3(b) and 3(c), we further present the individual contributions of the average ergotropy from the outputs $k = 1$ and $k \neq 1$, which are, respectively, defined by

$$\overline{W}_{k=1} = p_{k=1} W[\rho_{k=1}(\tau)] \quad \text{and} \quad \overline{W}_{k\neq1} = \sum_{k\neq1} p_k W[\rho_k(\tau)]. \tag{21}$$

We can observe that the inversion points come from the contribution of $k = 1$. Further, we can observe that its contribution decreases as N increases. When $N \geqslant 7$, the contribution vanishes for the entire charging period. In Appendix A, we provide analytical analysis, showing that the decrease in average ergotropy can also be attributed to the Zeno-type state freezing effect. More specifically, we demonstrate that the excited-state population for the postmeasurement state with $k = 1$ decreases when N increases. In the asymptotic limit ($N \to \infty$), the state can be frozen in the ground state. We further observe that the quick charging effect originates from the contribution of $k \neq 1$ since the corresponding average ergotropy becomes nonzero as soon as the charging process begins when $N > 2$.

However, in contrast to the previous results with the rotating-wave approximation, the average ergotropy cannot reach the upper bound even in the asymptotic limit, implying that the postmeasurement states are not pure. In Fig. 3(d), we present the average purity $\mathcal{P}$ associated with the postmeasurement states, which is defined by

$$\mathcal{P} = \sum_k \mathrm{Tr}[\sigma_k]\mathrm{Tr}\left[\left(\frac{\sigma_k}{\mathrm{Tr}[\sigma_k]}\right)^2\right]. \tag{22}$$

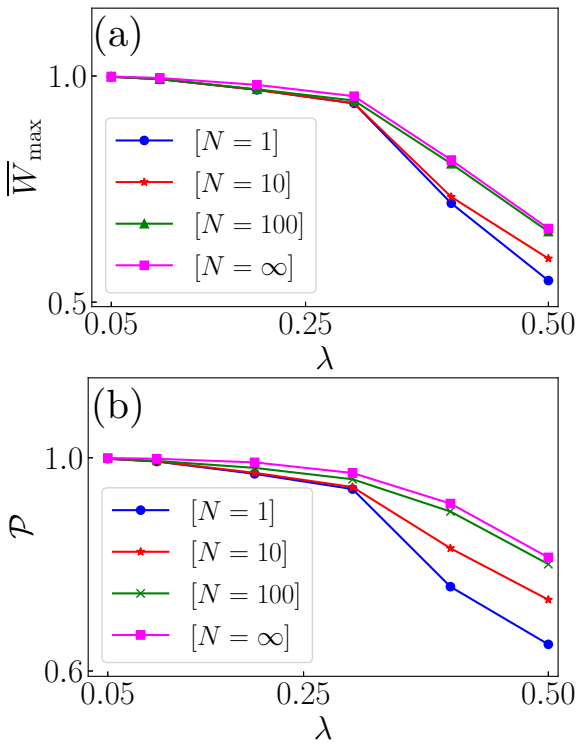

FIG. 4. (a) Maximum average ergotropy $\overline{W}_{\max}$ defined in Eq. (23) with respect to different coupling strength λ. The blue, red, green, and magenta dashed lines represent the results for $N = 1$, 10, 100, and ∞, respectively. (b) The average purity $\mathcal{P}$ on dimensionless coupling strength λ. The blue, red, green, and magenta dashed lines represent the results for $N = 1$, 10, 100, and ∞, respectively. The cutoff photon number is set to 9 in the above results.

We can observe the overall average purity increasing as N increases due to the Zeno-type effect, thereby leading to the enhancement of average ergotropy. However, the average purity cannot reach unity even in the asymptotic limit. Thus, the stored energy cannot be fully converted into extractable work. In Figs. 4(a) and 4(b), we compare the maximum average ergotropy with the average purity with respect to the coupling strength λ, where the maximum average ergotropy is defined by

$$\overline{W}_{\max} = \max_{\tau\in[0,T/4]} \overline{W}(\tau). \tag{23}$$

We can observe that as the coupling strength increases, the average purity drops, hence leading to a decrease in the maximum average ergotropy.

III. SINGLE-CHARGER PROTOCOL

In this section, we discuss the single-charger protocol as shown in Fig. 1(b), where the quantum battery can enter and interact with a single cavity (charger) C at different positions. The charging protocol resembles the one in Sec. II, albeit with two minor adjustments. First, we only use a single charger C instead of multiple ones. Second, the N-dimensional qudit D now acts as a quantum control that decides the QB's position of entry into C. More specifically, a path labeled by j guides the QB to a designated position denoted as r_j inside the cavity.

In this scenario, the QB experiences a varying coupling strength with respect to the position inside that charger [63]. Therefore, the position-dependent QB-charger Hamiltonian can be written as

$$H_j = H_Q + H_C + H'_j, \tag{24}$$

where $H_C = \hbar\omega_c \hat{a}^\dagger \hat{a}$. Here, H'_j represents the interaction Hamiltonian when QB is located at the position r_j. Its explicit form is given by

$$H'_j = \hbar\omega_c \lambda \cos\left(\pi \frac{r_j}{L}\right)\hat{\sigma}_x(\hat{a} + \hat{a}^\dagger), \tag{25}$$

where L denotes the width of the charger and λ represents the maximal QB-charger coupling strength, which can be achieved when $r_j = 0$ or L. Thus, the total Hamiltonian for this scenario can be expressed by

$$H_{\text{tot}} = \sum_{j=1}^{N} |j\rangle\langle j|_D \otimes H_j. \tag{26}$$

Similar to the previous consideration, we prepare the total system in the following initial state:

$$|\psi(0)\rangle_{DQC} = \frac{1}{\sqrt{N}} \sum_{j=1}^{N} |j\rangle_D \otimes |g\rangle_Q \otimes |1\rangle_C, \tag{27}$$

and allow it to evolve according to the total Hamiltonian H_{tot}, namely,

$$|\psi(\tau)\rangle_{DQC} = \frac{1}{\sqrt{N}} \sum_{j=1}^{N} |j\rangle_D \otimes |\phi_j(\tau)\rangle_{QC}, \tag{28}$$

where $|\phi_j(\tau)\rangle_{QC}$, in this case, is defined as

$$|\phi_j(\tau)\rangle_{QC} = \exp\left(-i\frac{\tau}{\hbar}H_j\right)(|g\rangle_Q \otimes |1\rangle_C). \tag{29}$$

We also consider the projectors defined in Eq. (7) to characterize the measurements performed by using MPBS2, such that the corresponding postmeasurement states read as

$$P_k |\psi(\tau)\rangle_{DQC} = |\xi_k\rangle_D \otimes \sum_{j=1}^{N} c_{k,j} |\phi_j(\tau)\rangle_{QC}, \tag{30}$$

where the coefficient $c_{k,j}$ is given by

$$c_{k,j} = \frac{1}{\sqrt{N}}\langle\xi_k|j\rangle. \tag{31}$$

We now switch to the interaction picture, such that the interaction Hamiltonian associated with the position r_j can be expressed as

$$\begin{aligned} H'_j(\tau) &= e^{\frac{i}{\hbar}(H_Q+H_C)\tau} H'_j e^{-\frac{i}{\hbar}(H_Q+H_C)\tau} \\ &= \cos\left(\pi \frac{r_j}{L}\right) H'_I(\tau), \end{aligned} \tag{32}$$

where $H'_I(\tau)$ is the position-independent part and reads as

$$H'_I(\tau) = \hbar\omega_c\lambda e^{\frac{i}{\hbar}(H_Q+H_C)\tau}\hat{\sigma}_x(\hat{a} + \hat{a}^\dagger)e^{-\frac{i}{\hbar}(H_Q+H_C)\tau}. \tag{33}$$

We can now characterize the time evolution with the propagator $U_{j,I}(\tau,0)$ in terms of the Dyson series, namely,

$$U_{j,I}(\tau,0) = \hat{\mathcal{T}} \exp\left[\frac{-i}{\hbar}\int_0^\tau H_j'(t')dt'\right] = \sum_{n=0}^{\infty}\frac{1}{n!}\left[-\frac{i}{\hbar}\cos\left(\pi\frac{r_j}{L}\right)\right]^n \times \int_0^\tau dt_1 \cdots \int_0^\tau dt_n \hat{\mathcal{T}} H_I'(t_1)\ldots H_I'(t_n), \quad (34)$$

where $\hat{\mathcal{T}}$ is the time-ordering operator with $t_1 > t_2 > \cdots > t_n$. The postmeasurement state of the QB and the charger in Eq. (30) can then be expressed by

$$\sum_{j=1}^{N} c_{k,j}\,|\phi_j(\tau)\rangle_{QC} = \sum_{j=1}^{N} c_{k,j} U_{j,I}(\tau,0)\,|g\rangle_Q \otimes |1\rangle_C\,. \quad (35)$$

Therefore, one can observe that the total evolution (including the qudit, the QB, and the charger) is described by a linear combination of the position-dependent propagators, which characterizes the collective quantum interference effect among different positions [54].

We now show that two superposed trajectories (positions) can lead to the saturation of the ergotropy to its upper bound with an appropriate adjustment of the Dicke-type interference effect. More specifically, we consider that the two positions satisfy $r_1 + r_2 = L$, such that

$$\cos\left(\pi\frac{r_2}{L}\right) = \cos\left(\pi - \pi\frac{r_1}{L}\right) = -\cos\left(\pi\frac{r_1}{L}\right). \quad (36)$$

Therefore, the coupling strengths share the same magnitude but are completely out of phase. Furthermore, we consider

$$|\xi_{k=1}\rangle = \frac{1}{\sqrt{2}}(|1\rangle_D + |2\rangle_D),$$
$$|\xi_{k=2}\rangle = \frac{1}{\sqrt{2}}(|1\rangle_D - |2\rangle_D), \quad (37)$$

and, according to Eq. (31), the coefficients in this case are

$$c_{1,1} = c_{1,2} = c_{2,1} = -c_{2,2} = \tfrac{1}{2}. \quad (38)$$

Therefore, the time evolution of the postmeasurement state of the QB and the charger for $k = 1$ is given by

$$\sum_{j=1}^{2} c_{1,j} U_{j,I}(\tau,0)\,|g\rangle_Q \otimes |1\rangle_C = \frac{1}{2}[U_{1,I}(\tau,0) + U_{2,I}(\tau,0)]\,|g\rangle_Q \otimes |1\rangle_C = \sum_{n\,\text{even}}^{\infty}\frac{1}{n!}\left[-\frac{i}{\hbar}\cos\left(\pi\frac{r_1}{L}\right)\right]^n \times \int_0^\tau dt_1 \cdots \int_0^\tau dt_n \hat{\mathcal{T}} H_I'(t_1)\ldots H_I'(t_n)\,|g\rangle_Q \otimes |1\rangle_C\,. \quad (39)$$

We can observe that in the Dyson series, all the odd terms vanish, leading to the phenomenon of destructive interference. This effect originates from the complete out-of-phase nature of the coupling strengths for the two positions. As a direct consequence, the QB remains in the ground state $|g\rangle$ throughout the entire process. Analogously, the postmeasurement state for $k = 2$ can be written as

$$\sum_{j=1}^{2} c_{2,j} U_{j,I}(\tau,0)\,|g\rangle_Q \otimes |1\rangle_C = \frac{1}{2}[U_{1,I}(\tau,0) - U_{2,I}(\tau,0)]\,|g\rangle_Q \otimes |1\rangle_C = \sum_{n\,\text{odd}}^{\infty}\frac{1}{n!}\left[-\frac{i}{\hbar}\cos\left(\pi\frac{r_1}{L}\right)\right]^n \times \int_0^\tau dt_1 \cdots \int_0^\tau dt_n \hat{\mathcal{T}} H_I'(t_1)\ldots H_I'(t_n)\,|g\rangle_Q \otimes |1\rangle_C\,. \quad (40)$$

In this case, all the even terms in the Dyson series vanish, implying the QB is in the excited state $|e\rangle$ for all $\tau > 0$ (with zero probability of obtaining the output $k = 2$ at $\tau = 0$). Notably, because the postmeasurement QB states for these two outputs are pure states (i.e., the average purity is one), we can conclude that the stored energy can be fully converted to the extractable work, i.e., $E = \overline{W}$, throughout the whole charging process. Note that the presented analysis does not rely on the rotating-wave approximation, thus indicating that the "perfect charging result" holds for all regimes of the QB-charger coupling strength.

It is worth emphasizing that achieving the perfect charging result only requires two superposed trajectories (positions). This indicates that a single-charger protocol emerges as a more experimentally feasible charging design with superior performance. In the subsequent sections, we delve into potential energy costs associated with various charging protocols and analyze the effects of scaling up the number of batteries. Our findings can reinforce that the single-charger protocol holds more advantages compared to the multiple-charger protocol.

IV. ENERGY COSTS OF THE QUANTUM CONTROL

As previously mentioned, the enhancement of ergotropy in the proposed protocols hinges on quantum control and its coherence. Notably, this may entail additional energy consumption, especially when considering energetic quantum control platforms such as the IBMQ and the IonQ experiments discussed below. In this section, we investigate two key aspects regarding potential energy consumption: The energy costs associated with (1) establishing the initial coherence and (2) the measurement.

A. Energy cost for creating coherence

Suppose that D is initialized in a state ρ_D and H_D is the corresponding Hamiltonian. The coherence can be induced by performing a unitary transformation V. According to Ref. [64], the work cost for generating coherence can be estimated by the change of D's internal energy, expressed as

$$W_{\text{coh}} = \text{Tr}[H_D(V\rho_D V^\dagger - \rho_D)]. \quad (41)$$

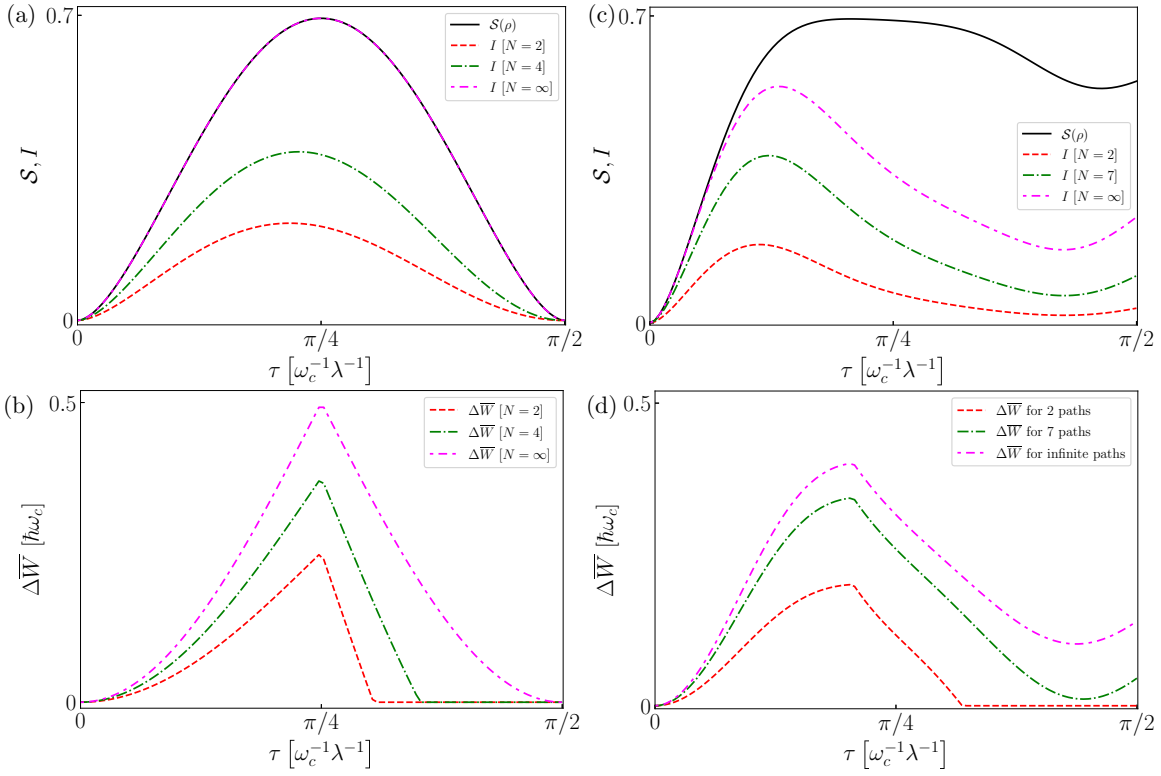

FIG. 5. Under the multiple-charger protocol, the numerical simulations for the von Neumann entropy of the premeasurement state $\mathcal{S}(\rho)$ and quantum-classical mutual information I with (a) $\lambda = 0.05$ and (c) $\lambda = 0.5$, and the ergotropy gain $\Delta\overline{W}$ with (b) $\lambda = 0.05$ and (d) $\lambda = 0.5$.

For the IBMQ and the IonQ experiments outlined in the following, we utilize a physical qubit as quantum control with a Hamiltonian $H_D = \hbar\omega_D\sigma_z/2$, where ω_D is the corresponding working frequency. The qubit is initialized in the ground state $|g\rangle_D$, and the target superposition (coherent) state is $(|g\rangle_D + |e\rangle_D)/\sqrt{2}$, achievable through a Hadamard transform. Consequently, the corresponding work cost is $\hbar\omega_D/2$. One can expect that the work cost increases proportionally with the dimension of D, i.e., the number of superposed trajectories. From this perspective, the single-charger protocol can be more advantageous than the multiple-charger protocol, as achieving perfect charging result in the former scenario requires only two trajectories, while the latter demands an infinite number of trajectories (and consequently infinite energy to create coherence) for achieving the perfect charging result.

B. Work cost for the measurement and the postselection

The proposed charging protocols also require the quantum control to serve as Maxwell's demon, where the energy required to perform the measurement and reset the demon's memory shall be taken into account. To this end, we adopt the framework proposed in Ref. [65], where the work costs for performing the measurement and resetting the memory can be characterized by the following relation:

$$W^M_{\text{meas}} + W^M_{\text{eras}} \geqslant k_B T I \tag{42}$$

with k_B being the Boltzmann constant and T representing the temperature of a thermal bath used to reset the memory. Thus, the work costs for the measurement W^M_{meas} together with the memory erasure W^M_{eras} are lower bounded by the quantum-classical mutual information I, which is defined by

$$I = \mathcal{S}(\rho) - \sum_k p(k)\mathcal{S}(\rho_k), \tag{43}$$

where $\mathcal{S}$ denotes the von Neumann entropy. Here, ρ denotes the premeasurement quantum state of the battery, while $p(k)$ represents the probability of obtaining the outcome k with a corresponding postmeasurement state ρ_k. Note that $I \leqslant S(\rho)$, and the upper limit is achieved when all the postmeasurement states are pure, i.e., $S(\rho_k) = 0\ \forall\ k$.

According to Eq. (42), we estimate the cost for the measurement through the quantum-classical mutual information in the following analysis. In Fig. 5, we showcase the quantum-classical mutual information and the ergotropy gain corresponding to the multiple-charger protocol. The ergotropy gain $\Delta\overline{W}$ is defined as the enhancement in the average ergotropy for multiple superposed trajectories ($N > 1$) compared to the case with $N = 1$:

$$\Delta\overline{W} \equiv \overline{W}[\tilde{N}] - \overline{W}[N = 1] \quad \text{with } \tilde{N} > 1. \tag{44}$$

In general, as we increase the number of superposed trajectories, I also increases, signifying an increase in the work cost associated with the measurement. Further, a comparison between the top and bottom figures reveals that ergotropy

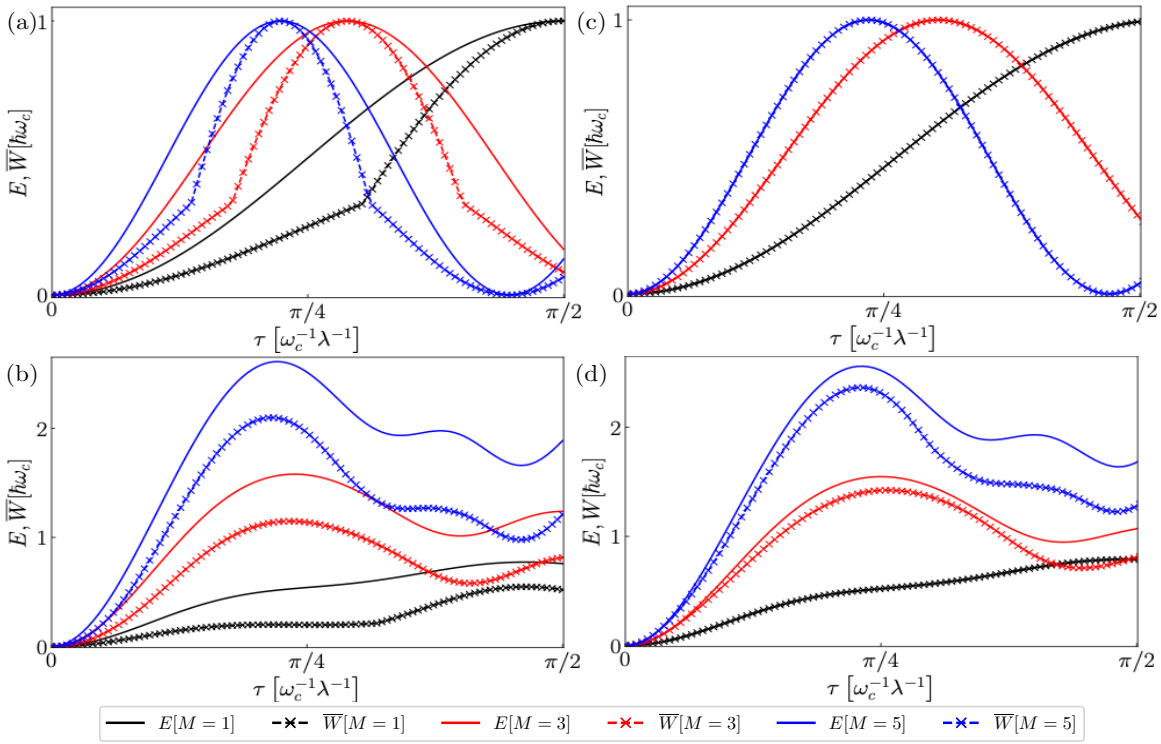

FIG. 6. The stored energy E and average ergotropy $\overline{W}$ for different numbers (M) of QBs under two superposed trajectories ($N = 2$) but different charging protocols. (a) Multiple-charger protocol with the coupling strength $\lambda = 0.05$. (b) Multiple-charger protocol with the coupling strength $\lambda = 0.5$. (c) Single-charger protocol with $r_1 = 0.1l$, $r_2 = 0.9l$, and the coupling strength $\lambda = 0.05$. (d) Single-charger protocol with $r_1 = 0.1l$, $r_2 = 0.9l$, and the coupling strength $\lambda = 0.5$. Note that the rotating-wave approximation is considered for (a) and (c).

enhancement through our protocol requires nonzero quantum-classical mutual information but not *vice versa*. As shown in Figs. 5(a) and 5(c), the quantum-classical mutual information remains nonzero throughout the entire charging time. Nevertheless, for the strong coupling case [Fig. 5(b)], the ergotropy gain diminishes after a finite charging period in cases with a finite number of superposed trajectories. In such instances, the information does not assist in work extraction, which suggests that the energy cost for the measurement becomes wasted. A similar situation can be observed for the ultrastrong coupling case [Fig. 5(d)], where seven superposed trajectories are required so that nonzero ergotropy gain can persist throughout the entire process. From this perspective, the single-charger protocol emerges as a more energy-efficient choice due to the "perfect charging effect", where nonzero ergotropy gain persists throughout the entirety of the charging process with only two superposed trajectories.

V. IMPACTS ON SCALING UP THE NUMBER OF BATTERIES

As reported in Ref. [11], collective charging for multiple quantum batteries can further accelerate the charging process. Here, we present numerical simulations for scaling up the number of the qubit batteries, revealing the interplay between the collective charging effect and the quick charging effect in the proposed protocols. Specifically, we modify the qubit-charger Hamiltonians for the multiple-charger and the single-charger protocols, which are, respectively, expressed by

$$H_{QC_j} = \hbar\omega_c \hat{a}_j^\dagger \hat{a}_j + \omega_a \hat{J}_z + 2\omega_c \lambda \hat{J}_x (\hat{a}_j^\dagger + \hat{a}_j),$$
$$H_j = \hbar\omega_c \hat{a}^\dagger \hat{a} + \omega_a \hat{J}_z + 2\omega_c \lambda \cos\left(\pi \frac{r_j}{L}\right) \hat{J}_x (\hat{a} + \hat{a}^\dagger). \tag{45}$$

Here, $\hat{J}_\alpha = (\hbar/2)\sum_i^N \hat{\sigma}_i^\alpha$ represents the components of the collective spin operator in terms of the Pauli operators for the ith QB. Initially, the batteries reside in their ground state, while each cavity charger harbors one photon. In Fig. 6, we present the results with two superposed trajectories ($N = 2$) for both the multiple-charger [Figs. 6(a) and 6(b)] and single-charger protocols [Figs. 6(c) and 6(d)]. As the number of batteries (M) increases, the charging of energy and ergotropy accelerates. This observation aligns with previous studies, suggesting that the collective effect of multiple quantum batteries can expedite charging processes [11]. In addition, the phenomenon of quick charging persists for both charging protocols, with ergotropy becoming available at the outset of the charging process. Furthermore, the available ergotropy for the single-charger protocol is generally larger than that for the multiple-charger protocol due to the additional superposition-induced Dicke-type interference effect [66]. Notably, in the strong coupling case for the single-charger protocol [Fig. 6(c)], the perfect charging effect persists in the multiple-battery scenario. These findings further enhance the potential utility of the single-charging protocol and the underlying superposition-induced Dicke-type interference

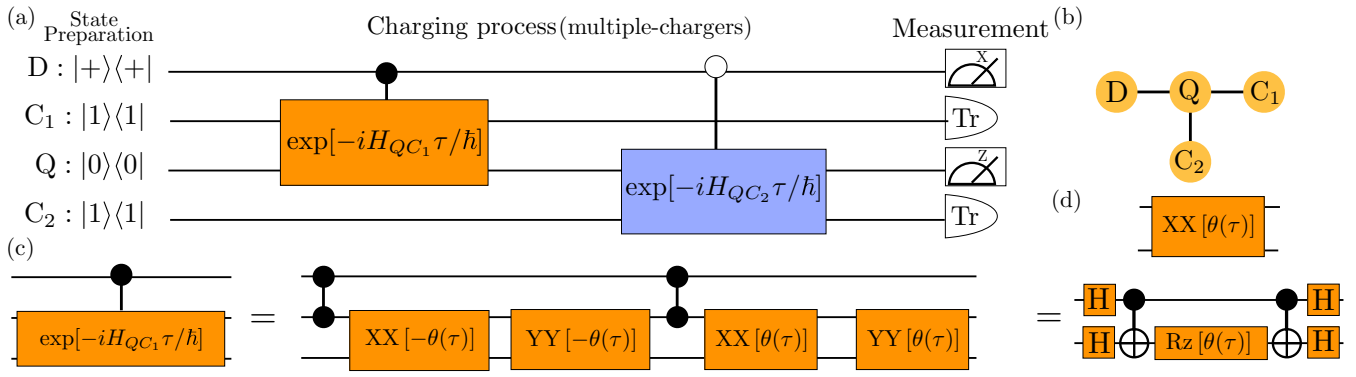

FIG. 7. (a) Quantum circuit for multiple-chargers protocol. Here, D, Q, C_1, C_2 represent the control qubit, battery qubit, first charger, and second charger, respectively. "Tr" is trace out. (b) Decomposition of a controlled unitary in (a). (c) Qubit configuration used on ibmq_algiers. (d) Decomposition of a XX gate into CNOT gates.

effect. Finally, we remark that for the ultrastrong coupling case [Figs. 6(b) and 6(d)], the results indicate not only the acceleration of the charging process but also an increase in the amount of energy stored in the batteries. This originates from the breakdown of excitation conservation when the coupling strength between the batteries and the chargers is sufficiently strong.

VI. IMPLEMENTATION ON QUANTUM DEVICES

In this section, we provide circuit models for the proposed charging protocols and perform proof-of-concept experiments on the quantum processors provided by IBMQ and IonQ, which involves two superposed trajectories ($N = 2$).

The quantum circuit for the multiple-charging setup is described by Fig. 7(a). The circuit consists of four qubits, representing the control qubit D, the quantum battery Q, and the two charging cavities C_1 and C_2, respectively. The circuit can be divided into three parts: state preparation, charging process, and measurements on the control qubit and quantum battery. In the state preparation part, the qubits are prepared in the initial state specified in Eq. (4) using single-qubit gates. The charging process involves the utilization of two controlled-unitary gates to simulate the simultaneous charging of the qubit by the two cavities through Jaynes-Cummings interactions. In Fig. 7(b), we present the decomposition of the controlled unitaries into bit-flip (X) gates, controlled-z gates (CZ), and Ising coupling gates [$XX(\theta)$ and $YY(\theta)$], defined as follows:

$$\begin{aligned} X &= \hat{\sigma}_x, \\ CZ &= |0\rangle\langle 0| \otimes \mathbb{1} + |1\rangle\langle 1| \otimes \hat{\sigma}_z, \\ XX(\theta) &= \cos(\theta/2)\mathbb{1} \otimes \mathbb{1} - i\sin(\theta/2)\hat{\sigma}_x \otimes \hat{\sigma}_x, \\ YY(\theta) &= \cos(\theta/2)\mathbb{1} \otimes \mathbb{1} - i\sin(\theta/2)\hat{\sigma}_y \otimes \hat{\sigma}_y. \end{aligned} \tag{46}$$

Here, we map the charging time τ into the angle θ using the following relation:

$$\theta(\tau) = \omega_c \lambda \tau/2. \tag{47}$$

Finally, in the measurement part, we measure the control qubit D in the x direction, aligned with the projectors described by Eq. (37). Furthermore, as indicated in Eq. (19), the QB's postmeasurement states are diagonalized under the energy eigenstates. Consequently, we can only measure Q in the z direction to determine the stored energy as well as the ergotropy. We utilize the ibmq_algiers and IonQ-Aria 1 devices. Note that the qubit configuration for ibmq_algiers is illustrated in Fig. 7(c), while the qubits in IonQ-Aria 1 are fully connected. Also, since the Ising coupling gates are not native gates for the IBMQ device, we need to further decompose them into CNOT gates, which is shown in Fig. 7(d). Consequently, the circuits for the IBMQ and IonQ devices consist of 20 and 12 two-qubit gates, respectively. Here, we use the Hadamard (H) gate and the rotation-z [$R_z(\theta)$] gate, which are defined by

$$\begin{aligned} H &= \frac{1}{2}\begin{pmatrix} 1 & 1 \\ 1 & -1 \end{pmatrix}, \\ R_z(\theta) &= \exp(-i\hat{\sigma}_z\theta/2). \end{aligned} \tag{48}$$

For the single-charger setup, the circuit model for the charging process is presented in Fig. 8, which consists of 6 and 4 two-qubit gates in the circuits for the IBMQ and the IonQ devices, respectively.

Figures 9 and 10 illustrate the results obtained from the two protocols, with each data point representing the average of 1000 experiment repetitions. The experimental results demonstrate a notable increase in average ergotropy, aligning with the theoretical predictions. Furthermore, we can observe that the deviation between the experimental and theoretical results is correlated by the circuit size, primarily determined by the number of two-qubit gates involved. Therefore, comparing the results from the IonQ and IBMQ devices, we find that the experimental data from the IonQ device exhibit a closer match to the theoretical curves compared to those from the IBMQ device. In addition, the errors associated with the

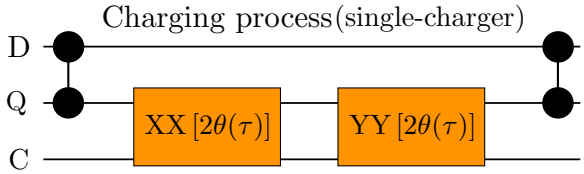

FIG. 8. Charging process of the single-charger setup, where the coupling strengths of the two superposed trajectories have the same magnitude but are out of phase.

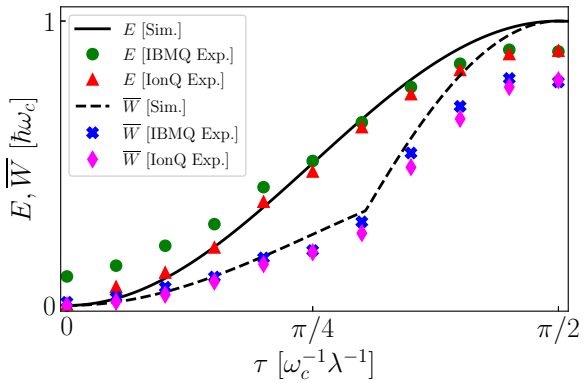

FIG. 9. The stored energy E and average ergotropy $\overline{W}$ (both in units of $\hbar\omega_c$) on time τ (in units of $1/\omega_c$) for $\lambda = 0.05, N = 2$. The black solid and dashed curves represent the stored energy and average ergotorpy predicted by numerical simulations. The green circles and blue "x"s represent experimental results performed on ibmq_algiers. The red triangles and magenta diamonds represent experimental results performed on IonQ Aria 1. Each data point is obtained after averaging 1000 experimental repetitions.

single-charger protocol are smaller in magnitude than those of the multiple-charger protocol. Finally, we remark that when observing the experimental results for the stored energy, the errors for the cases $\tau = 0$ and $\pi/2$ are larger compared to the case $\tau = \pi/4$. This can be attributed to the depolarizing noise (i.e., gate error), which is modeled by incoherently mixing the ideal system's state with the maximally mixed state [67]. At the times $\tau = 0$ and $\pi/2$, the ideal battery states are, respectively, $|g\rangle$ and $|e\rangle$, where the corresponding stored energies are $E = 0$ and $\hbar\omega_a$. When mixing the maximally mixed state for these cases, the stored energy, respectively, become larger and smaller than the ideal results. However, for the ideal case, the battery is already in the maximally mixed state, i.e., $(|g\rangle\langle g| + |e\rangle\langle e|)/2$ at the time $\tau = \pi/4$. Consequently, the

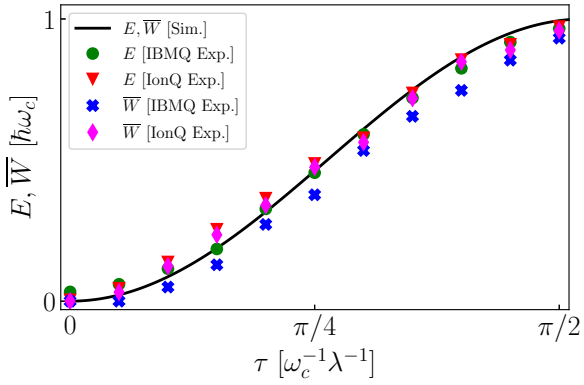

FIG. 10. The stored energy E and average ergotropy $\overline{W}$ (both in units of $\hbar\omega_c$) on time τ (in units of $1/\omega_c$) with $r_1 = 0.1l$ and $r_2 = 0.9l$. The black curve represents the stored energy and average ergotropy predicted by numerical simulations. The green circle and blue "x"s represent the experimental results performed on ibmq_algiers. The red triangles and magenta diamonds represent experimental results performed on IonQ Aria 1. Each data point is obtained after averaging 1000 experimental repetitions.

depolarizing noise does not change the battery's state, leaving the stored energy unchanged. Therefore, by taking the gate error into account, the results for $\tau = 0$ and $\pi/2$ demonstrate a larger error compared to the result for $\tau = \pi/4$.

VII. SUMMARY AND OUTLOOK

In this work, we utilize superposition of trajectories to propose two charging protocols (i.e., the multiple-charger protocol and the single-charger protocol) for quantum batteries (QBs), leading to quick charging effect of extractable work (ergotropy). We prove that the increase in ergotropy arises from the initial coherence of the quantum control. In addition, upon examining the potential resource consumption, we determine that the single-charger protocol, demonstrating the perfect charging effect through the utilization of collective interference, presents a superior scenario compared to the multiple-charger protocol. We further illustrate that this advantage persists even when scaling up the number of QBs. Moreover, we investigate the circuit implementations utilizing IonQ and IBMQ devices, providing experimental data that further support the enhanced extractable work, thus validating our theoretical predictions.

As a possible future direction, we could extend our charging protocols to a related framework called indefinite causal order [68–73], which allows for the control of quantum operation ordering through a quantum switch. Based on this framework, we could consider the scenarios, where the ordering of the charging process becomes indefinite [74–77]. This exploration could shed light on the potential benefits and implications of incorporating indefinite causal order into our proposed protocols, further advancing the field of quantum battery charging.

ACKNOWLEDGMENTS

We acknowledge the NTU-IBM Q Hub, IBM quantum experience, and Cloud Computing Center for Quantum Science & Technology at NCKU for providing us a platform to implement the experiment. This work is supported by the National Center for Theoretical Sciences and National Science and Technology Council, Taiwan, Grants No. NSTC 112-2123-M-006-001 and No. NSTC 112-2119-M-006-010.

APPENDIX A: EFFECTS OF THE CHOICE OF PROJECTORS ON THE POSTMEASUREMENT QUANTUM BATTERY STATES

Here, we prove that the choice of projectors for $|\xi_{k\neq1}\rangle\langle\xi_{k\neq1}|_D$ is irrelevant to the postmeasurement states $\sigma_{k\neq1}(\tau)$ as long as they are orthonormal to $|\xi_{k=1}\rangle\langle\xi_{k=1}|_D$.

Let us start from Eq. (8), which can be expanded into

$$\sigma_k(\tau) = \frac{1}{N}\sum_{j,f=1}^{N}\langle\xi_k|j\rangle\langle f|\xi_k\rangle\,\mathrm{Tr}_C[|\phi_j(\tau)\rangle\langle\phi_f(\tau)|_{QC}]. \tag{A1}$$

We switch to the interaction picture, where the interaction Hamiltonian reads as

$$H'_{QC_j}(\tau) = e^{\frac{i}{\hbar}(H_Q+H_{C_j})\tau} H'_{QC_j} e^{-\frac{i}{\hbar}(H_Q+H_{C_j})\tau}. \tag{A2}$$

The time-dependent part of postmeasurement states can be generally expressed by

$$|\phi_j(\tau)\rangle_{QC} = \sum_{n=0}^{\infty} \alpha_n(\tau)\,|n_j\rangle\,, \tag{A3}$$

with

$$|n_j\rangle = (\hat{\sigma}_x)^n\,|e\rangle \otimes \frac{(\hat{a}_j^\dagger)^n \hat{a}_j}{\sqrt{n!}} \bigotimes_{m=1}^{N} |1\rangle_{C_m}\,. \tag{A4}$$

Note that in the following analysis, we show the explicit expression of the time-dependent coefficient $\alpha_n(\tau)$ does not affect the result. Thus, we will keep them unspecified. Now, we can show that

$$\begin{aligned}&\mathrm{Tr}_C[|\phi_j(\tau)\rangle\langle\phi_f(\tau)|_{QC}] \\ &= \begin{cases} \sum_{n=0}^{\infty} |\alpha_n(\tau)|^2 \sigma_x^n\,|e\rangle\langle e|\,\sigma_x^n & \text{for } j=f, \\ |\alpha_1(\tau)|^2\,|g\rangle\langle g| & \text{for } j\neq f. \end{cases}\end{aligned} \tag{A5}$$

Inserting this into Eq. (A1), we can obtain

$$\begin{aligned}\sigma_k(\tau) = &\sum_{n=0}^{\infty} |\alpha_n(\tau)|^2 \sigma_x^n\,|e\rangle\langle e|\,\sigma_x^n \frac{1}{N}\sum_{j=f}^{N} |\langle\xi_k|j\rangle|^2 \\ &+ |\alpha_1(\tau)|^2\,|g\rangle\langle g| \frac{1}{N}\sum_{j\neq f}^{N}\sum_{f=1}^{N} \langle\xi_k|j\rangle\langle f|\xi_k\rangle\,.\end{aligned} \tag{A6}$$

For the case of $k=1$, according to Eq. (7), we can obtain

$$\langle\xi_{k=1}|j\rangle = \frac{1}{\sqrt{N}} \quad \forall\ j=1,\ldots,N. \tag{A7}$$

Therefore, the corresponding postmeasurement state can be written as

$$\begin{aligned}\sigma_{k=1}(\tau) = &\frac{1}{N}\sum_{n=0}^{\infty} |\alpha_n(\tau)|^2 \sigma_x^n\,|e\rangle\langle e|\,\sigma_x^n \\ &+ \frac{N-1}{N}|\alpha_1(\tau)|^2\,|g\rangle\langle g|\,.\end{aligned} \tag{A8}$$

Note that in the asymptotic limit ($N\to\infty$), we observe $\sigma_{k=1}(\tau)\propto|g\rangle\langle g|$, indicating the Zeno-type state freezing effect [54].

Recall that for the case of $k\neq 1$, we require the projectors to be orthonormal to that of $k=1$, i.e., $\langle\xi_{k\neq1}|\xi_{k=1}\rangle=0$, implying that the ket $|\xi_{k\neq1}\rangle$ can be expressed by

$$|\xi_{k\neq1}\rangle = \sum_{j=1}^{N}\beta_{k,j}\,|j\rangle_D\,, \quad \text{with} \quad \sum_{j=1}^{N}\beta_{k,j}=0 \ \ \forall\ k\neq1. \tag{A9}$$

Therefore, the postmeasurement states can be written as

$$\begin{aligned}\sigma_{k\neq1}(\tau) = &\frac{1}{N}\sum_{n=0}^{\infty} |\alpha_n(\tau)|^2 \sigma_x^n\,|e\rangle\langle e|\,\sigma_x^n \\ &- \frac{1}{N}|\alpha_1(\tau)|^2\,|g\rangle\langle g|\,.\end{aligned} \tag{A10}$$

This concludes the proof that the postmeasurement states are independent of the explicit expression of the coefficients $\beta_{k,j}$ associated with the projectors.

APPENDIX B: RELATION BETWEEN THE AVERAGE ERGOTROPY AND THE AVERAGE PURITY

Here, we show that an increase in average purity implies an increase in the average ergotropy. In this work, we mainly focus on a qubit battery, whose quantum state can be expressed as

$$\rho = \tfrac{1}{2}(\mathbb{1} + \vec{v}\cdot\vec{\sigma}), \tag{B1}$$

where $\vec{v}=(v_x,v_y,v_z)^T$ denotes the Bloch vector and $\vec{\sigma}=(\hat{\sigma}_x,\hat{\sigma}_y,\hat{\sigma}_z)^T$ represents a vector of Pauli matrices. In this representation, the passive state is given by

$$\varphi = \tfrac{1}{2}(\mathbb{1} - |\vec{v}|\hat{\sigma}_z). \tag{B2}$$

This corresponds to rotating the Bloch vector of ρ into a vector that aligns with the negative-z axis of the Bloch sphere. The ergotropy can then be expressed as

$$W(\rho) = \frac{\hbar\omega_c}{2}(v_z + |\vec{v}|). \tag{B3}$$

Given that the purity of ρ is $(1+|\vec{v}|^2)/2$, we can conclude that an increase in purity leads to an increase in ergotropy. This argument also holds for the average ergotropy, where the average ergotorpy and the average purity are expressed as

$$\begin{aligned}\overline{W} &= \sum_k p_k W(\rho_k) = \frac{\hbar\omega_c}{2}\left(v_z + \sum_k p_k|\vec{v}_k|\right), \\ \mathcal{P} &= \left(1+\sum_k p_k|\vec{v}_k|^2\right)\Big/2.\end{aligned} \tag{B4}$$

Thus, we can conclude that an increase in average purity also suggests an increase in the average ergotropy.

APPENDIX C: PROOF OF THE PROPOSITION: QUANTUM COHERENCE IS A NECESSARY RESOURCE FOR THE ERGOTROPY GAIN

We now delve into the details of the proof outlined in the main text. We start by considering an N-dimensional control qudit D initialized in a general quantum state:

$$\rho_D = \sum_{j=1}^{N} x_j\,|j\rangle\langle j|_D + \sum_{j\neq f} y_{jf}\,|j\rangle\langle f|_D\,, \tag{C1}$$

where x_j and y_{jf} represent the diagonal and off-diagonal (coherence) terms of ρ_D, respectively. For the multiple-charger protocol, the temporal evolution of the total state is written as

$$\begin{aligned}\rho_{DQC} = &\sum_{j=1}^{N} x_j\,|j\rangle\langle j|_D \otimes |\phi_j(\tau)\rangle\langle\phi_j(\tau)|_{QC} \\ &+ \sum_{j\neq f} y_{jf}\,|j\rangle\langle f|_D \otimes |\phi_j(\tau)\rangle\langle\phi_f(\tau)|_{QC}\,,\end{aligned} \tag{C2}$$

where $|\phi_j(\tau)\rangle_{QC}$ is described in Eq. (A3). By tracing out the chargers (cavities), we obtain

$$\rho_{DQ} = \sum_{j=1}^{N} x_j \, |j\rangle\langle j|_D \otimes [\alpha \, 0|e\rangle\langle e|_Q + (1-\alpha)\,|g\rangle\langle g|_Q] + \sum_{j\neq f} y_{jf}\,|j\rangle\langle f|_D \otimes \beta\,|g\rangle\langle g|_Q\,, \tag{C3}$$

where $\alpha = \sum_{n,\text{even}}^{\infty} |\alpha_n(\tau)|^2$, $1-\alpha = \sum_{n,\text{odd}}^{\infty} |\alpha_n(\tau)|^2$, and $\beta = |\alpha_1(\tau)|^2$.

The key insight is that if the initial control qudit is incoherent, i.e., $y_{jf} = 0 \;\forall\; j \neq f$, the control and the battery ρ_{DQ} becomes completely uncorrelated, namely, $\rho_{DQ} = \rho_D \otimes \rho_Q$ with $\rho_D = \sum_{j=1}^{N} x_j\,|j\rangle\langle j|_D$ and $\rho_Q = [\alpha\,|e\rangle\langle e|_Q + (1-\alpha)\,|g\rangle\langle g|_Q]$. Consequently, irrespective of the number of trajectories N or the measurement basis, we arrive at the same battery state $\rho_Q(\tau)$, which is also identical to the scenario with a single charger $N = 1$. This implies that in the absence of coherence, the battery fails to exhibit the quick charging effect. The proof is completed, and we assert that coherence serves as an indispensable resource for the quick charging phenomenon in the multiple-charger protocol. Furthermore, employing the same methodology, we can easily conclude that the initial coherence of the control qudit is equally essential in the single-charger protocol.

We now focus on our scenarios, where the off-diagonal terms of ρ_D are identical. We introduce a parameter $0 \leqslant \epsilon \leqslant 1$ for tuning the initial coherence of the control qudit and make the amount of coherence become proportional to ϵ, i.e., $x_j = 1/N \;\forall\; j$ and $y_{jf} = \epsilon/N \;\forall\; j \neq f$. Therefore, the corresponding state is given by

$$\rho_D = \frac{1}{N}\sum_{j=1} |j\rangle\langle j|_D + \frac{\epsilon}{N}\sum_{j\neq f} |j\rangle\langle f|\,. \tag{C4}$$

In this case, the unnormalized postmeasurement states are expressed as

$$\sigma_{k=1} = \frac{1}{N}[\alpha\,|e\rangle\langle e| + (1-\alpha)\,|g\rangle\langle g|] + \frac{\epsilon}{N}(N-1)\beta\,|g\rangle\langle g|\,,$$
$$\sigma_{k\neq 1} = \frac{1}{N}[\alpha\,|e\rangle\langle e| + (1-\alpha)\,|g\rangle\langle g|] - \frac{\epsilon}{N}\beta\,|g\rangle\langle g|\,. \tag{C5}$$

To reveal the connection between the coherence and the ergotropy enhancement, we introduce the ergotropy gain for $\tilde{N}$ superposed trajectories, which is defined as

$$\Delta\overline{W} \equiv \overline{W}\big[\tilde{N}\big] - \overline{W}[N=1] \quad \text{with } \tilde{N} > 1. \tag{C6}$$

As indicated in the main text, in the region where the quick charging effect occurs (i.e., $\Delta\overline{W} > 0$), the nonzero ergotropy is contributed by $\sigma_{k\neq 1}$, such that

$$\overline{W}[\tilde{N}] = \frac{N-1}{N}\hbar\omega(2\alpha + \epsilon\beta - 1). \tag{C7}$$

The ergotropy gain can then be expressed as

$$\Delta\overline{W} = \begin{cases} \frac{N-1}{N}\hbar\omega\beta\,\epsilon + \frac{N-1}{N}\hbar\omega(2\alpha-1) & \text{for } \alpha \leqslant \frac{1}{2}, \\ \frac{N-1}{N}\hbar\omega\beta\,\epsilon - \frac{1}{N}\hbar\omega(2\alpha-1) & \text{for } \alpha \geqslant \frac{1}{2}. \end{cases} \tag{C8}$$

Therefore, we can conclude that the ergotropy gain is linearly proportional to the initial coherence in the control qudit.

[1] R. Uzdin, A. Levy, and R. Kosloff, Equivalence of quantum heat machines, and quantum-thermodynamic signatures, Phys. Rev. X **5**, 031044 (2015).

[2] W. Niedenzu, V. Mukherjee, A. Ghosh, A. G. Kofman, and G. Kurizki, Quantum engine efficiency bound beyond the second law of thermodynamics, Nat. Commun. **9**, 165 (2018).

[3] G. Gemme, M. Grossi, D. Ferraro, S. Vallecorsa, and M. Sassetti, IBM quantum platforms: A quantum battery perspective, Batteries **8**, 43 (2022).

[4] H.-L. Shi, S. Ding, Q.-K. Wan, X.-H. Wang, and W.-L. Yang, Entanglement, coherence, and extractable work in quantum batteries, Phys. Rev. Lett. **129**, 130602 (2022).

[5] R. Horodecki, P. Horodecki, M. Horodecki, and K. Horodecki, Quantum entanglement, Rev. Mod. Phys. **81**, 865 (2009).

[6] D. Bruß, Characterizing entanglement, J. Math. Phys. **43**, 4237 (2002).

[7] A. Streltsov, G. Adesso, and M. B. Plenio, Colloquium: Quantum coherence as a resource, Rev. Mod. Phys. **89**, 041003 (2017).

[8] O. Nairz, M. Arndt, and A. Zeilinger, Quantum interference experiments with large molecules, Am. J. Phys. **71**, 319 (2003).

[9] F. C. Binder, S. Vinjanampathy, K. Modi, and J. Goold, Quantacell: powerful charging of quantum batteries, New J. Phys. **17**, 075015 (2015).

[10] F. Campaioli, F. A. Pollock, F. C. Binder, L. Céleri, J. Goold, S. Vinjanampathy, and K. Modi, Enhancing the charging power of quantum batteries, Phys. Rev. Lett. **118**, 150601 (2017).

[11] D. Ferraro, M. Campisi, G. M. Andolina, V. Pellegrini, and M. Polini, High-power collective charging of a solid-state quantum battery, Phys. Rev. Lett. **120**, 117702 (2018).

[12] T. P. Le, J. Levinsen, K. Modi, M. M. Parish, and F. A. Pollock, Spin-chain model of a many-body quantum battery, Phys. Rev. A **97**, 022106 (2018).

[13] D. Rossini, G. M. Andolina, and M. Polini, Many-body localized quantum batteries, Phys. Rev. B **100**, 115142 (2019).

[14] D. Rossini, G. M. Andolina, D. Rosa, M. Carrega, and M. Polini, Quantum advantage in the charging process of Sachdev-Ye-Kitaev batteries, Phys. Rev. Lett. **125**, 236402 (2020).

[15] A. Crescente, M. Carrega, M. Sasetti, and D. Ferraro, Charging and energy fluctuations of a driven quantum battery, New J. Phys. **22**, 063057 (2020).

[16] A. Crescente, M. Carrega, M. Sassetti, and D. Ferraro, Ultrafast charging in a two-photon Dicke quantum battery, Phys. Rev. B **102**, 245407 (2020).

[17] S. Ghosh, T. Chanda, S. Mal, and A. Sen(De), Fast charging of a quantum battery assisted by noise, Phys. Rev. A **104**, 032207 (2021).

[18] J.-Y. Gyhm, D. Šafránek, and D. Rosa, Quantum charging advantage cannot be extensive without global operations, Phys. Rev. Lett. **128**, 140501 (2022).

[19] C. Rodríguez, D. Rosa, and J. Olle, Artificial intelligence discovery of a charging protocol in a micromaser quantum battery, Phys. Rev. A **108**, 042618 (2023).

[20] A. C. Santos, B. Çakmak, S. Campbell, and N. T. Zinner, Stable adiabatic quantum batteries, Phys. Rev. E **100**, 032107 (2019).
[21] F. Pirmoradian and K. Mølmer, Aging of a quantum battery, Phys. Rev. A **100**, 043833 (2019).
[22] J. Liu, D. Segal, and G. Hanna, Loss-free excitonic quantum battery, J. Phys. Chem. C **123**, 18303 (2019).
[23] J. Q. Quach and W. J. Munro, Using dark states to charge and stabilize open quantum batteries, Phys. Rev. Appl. **14**, 024092 (2020).
[24] S. Gherardini, F. Campaioli, F. Caruso, and F. C. Binder, Stabilizing open quantum batteries by sequential measurements, Phys. Rev. Res. **2**, 013095 (2020).
[25] D. Rosa, D. Rossini, G. M. Andolina, M. Polini, and M. Carrega, Ultra-stable charging of fast-scrambling SYK quantum batteries, J. High Energy Phys. 11 (2020) 067.
[26] X. Yang, Y.-H. Yang, M. Alimuddin, R. Salvia, S.-M. Fei, L.-M. Zhao, S. Nimmrichter, and M.-X. Luo, Battery capacity of energy-storing quantum systems, Phys. Rev. Lett. **131**, 030402 (2023).
[27] R. Alicki and M. Fannes, Entanglement boost for extractable work from ensembles of quantum batteries, Phys. Rev. E **87**, 042123 (2013).
[28] G. Francica, J. Goold, F. Plastina, and M. Paternostro, Daemonic ergotropy: enhanced work extraction from quantum correlations, npj Quantum Inf. **3**, 12 (2017).
[29] G. Manzano, F. Plastina, and R. Zambrini, Optimal work extraction and thermodynamics of quantum measurements and correlations, Phys. Rev. Lett. **121**, 120602 (2018).
[30] G. M. Andolina, M. Keck, A. Mari, M. Campisi, V. Giovannetti, and M. Polini, Extractable work, the role of correlations, and asymptotic freedom in quantum batteries, Phys. Rev. Lett. **122**, 047702 (2019).
[31] F. Barra, Dissipative charging of a quantum battery, Phys. Rev. Lett. **122**, 210601 (2019).
[32] G. Francica, F. C. Binder, G. Guarnieri, M. T. Mitchison, J. Goold, and F. Plastina, Quantum coherence and ergotropy, Phys. Rev. Lett. **125**, 180603 (2020).
[33] F. H. Kamin, F. T. Tabesh, S. Salimi, F. Kheirandish, and A. C. Santos, Non-Markovian effects on charging and self-discharging process of quantum batteries, New J. Phys. **22**, 083007 (2020).
[34] J. Monsel, M. Fellous-Asiani, B. Huard, and A. Auffèves, The energetic cost of work extraction, Phys. Rev. Lett. **124**, 130601 (2020).
[35] S. Ghosh, T. Chanda, and A. Sen(De), Enhancement in the performance of a quantum battery by ordered and disordered interactions, Phys. Rev. A **101**, 032115 (2020).
[36] G. Francica, Quantum correlations and ergotropy, Phys. Rev. E **105**, L052101 (2022).
[37] D. Šafránek, D. Rosa, and F. C. Binder, Work extraction from unknown quantum sources, Phys. Rev. Lett. **130**, 210401 (2023).
[38] K. Mei and J. Fang, Superabsorption-a method to improve absorbing boundary conditions (electromagnetic waves), IEEE Trans. Antennas Propag. **40**, 1001 (1992).
[39] K. D. B. Higgins, S. C. Benjamin, T. M. Stace, G. J. Milburn, B. W. Lovett, and E. M. Gauger, Superabsorption of light via quantum engineering, Nat. Commun. **5**, 4705 (2014).
[40] J. Q. Quach, K. E. McGhee, L. Ganzer, D. M. Rouse, B. W. Lovett, E. M. Gauger, J. Keeling, G. Cerullo, D. G. Lidzey, and T. Virgili, Superabsorption in an organic microcavity: Toward a quantum battery, Sci. Adv. **8**, eabk3160 (2022).
[41] J. Joshi and T. S. Mahesh, Experimental investigation of a quantum battery using star-topology nmr spin systems, Phys. Rev. A **106**, 042601 (2022).
[42] G. Gemme, G. M. Andolina, F. M. D. Pellegrino, M. Sassetti, and D. Ferraro, Off-resonant dicke quantum battery: Charging by virtual photons, Batteries **9**, 197 (2023).
[43] R. H. Dicke, Coherence in spontaneous radiation processes, Phys. Rev. **93**, 99 (1954).
[44] D. Yang, S.-h. Oh, J. Han, G. Son, J. Kim, J. Kim, M. Lee, and K. An, Realization of superabsorption by time reversal of superradiance, Nat. Photonics **15**, 272 (2021).
[45] Y. Ueki, S. Kamimura, Y. Matsuzaki, K. Yoshida, and Y. Tokura, Quantum battery based on superabsorption, J. Phys. Soc. Jpn. **91**, 124002 (2022).
[46] G. Chiribella and H. Kristjánsson, Quantum Shannon theory with superposition of trajectories, Proc. R. Soc. A. **475**, 20180903 (2019).
[47] J. Foo, S. Onoe, and M. Zych, Unruh-DeWitt detectors in quantum superpositions of trajectories, Phys. Rev. D **102**, 085013 (2020).
[48] H. Kristjánsson, G. Chiribella, S. Salek, D. Ebler, and M. Wilson, Resource theories of communication, New J. Phys. **22**, 073014 (2020).
[49] Q. Duprey and A. Matzkin, Proposal to observe path superpositions in a double-slit setup, Phys. Rev. A **105**, 052231 (2022).
[50] F. Ghafari, N. Tischler, C. Di Franco, J. Thompson, M. Gu, and G. J. Pryde, Interfering trajectories in experimental quantum-enhanced stochastic simulation, Nat. Commun. **10**, 1630 (2019).
[51] G. Rubino, L. A. Rozema, D. Ebler, H. Kristjánsson, S. Salek, P. Allard Guérin, A. A. Abbott, C. Branciard, Č. Brukner, G. Chiribella, and P. Walther, Experimental quantum communication enhancement by superposing trajectories, Phys. Rev. Res. **3**, 013093 (2021).
[52] J. Foo, S. Onoe, R. B. Mann, and M. Zych, Thermality, causality, and the quantum-controlled Unruh–deWitt detector, Phys. Rev. Res. **3**, 043056 (2021).
[53] F.-J. Chan, Y.-T. Huang, J.-D. Lin, H.-Y. Ku, J.-S. Chen, H.-B. Chen, and Y.-N. Chen, Maxwell's two-demon engine under pure dephasing noise, Phys. Rev. A **106**, 052201 (2022).
[54] J.-D. Lin, C.-Y. Huang, N. Lambert, G.-Y. Chen, F. Nori, and Y.-N. Chen, Space-time dual quantum Zeno effect: Interferometric engineering of open quantum system dynamics, Phys. Rev. Res. **4**, 033143 (2022).
[55] J.-D. Lin and Y.-N. Chen, Boosting entanglement growth of many-body localization by superpositions of disorder, Phys. Rev. A **108**, 022203 (2023).
[56] H.-Y. Ku, K.-Y. Lee, P.-R. Lai, J.-D. Lin, and Y.-N. Chen, Coherent activation of a steerability-breaking channel, Phys. Rev. A **107**, 042415 (2023).
[57] K.-Y. Lee, J.-D. Lin, A. Miranowicz, F. Nori, H.-Y. Ku, and Y.-N. Chen, Steering-enhanced quantum metrology using superpositions of noisy phase shifts, Phys. Rev. Res. **5**, 013103 (2023).
[58] B. Misra and E. G. Sudarshan, The Zeno's paradox in quantum theory, J. Math. Phys. **18**, 756 (1977).
[59] H.-P. Breuer and F. Petruccione, *The Theory of Open Quantum Systems* (Oxford University Press, Oxford, 2002).

[60] D. Morrone, M. A. Rossi, and M. G. Genoni, Daemonic ergotropy in continuously-monitored open quantum batteries, Phys. Rev. Appl. **20**, 044073 (2023).

[61] D. Meschede, H. Walther, and G. Müller, One-atom maser, Phys. Rev. Lett. **54**, 551 (1985).

[62] A. F. Kockum, A. Miranowicz, S. D. Liberato, S. Savasta, and F. Nori, Ultrastrong coupling between light and matter, Nat. Rev. Phys. **1**, 19 (2019).

[63] W. E. Shanks, D. L. Underwood, and A. A. Houck, A scanning transmon qubit for strong coupling circuit quantum electrodynamics, Nat. Commun. **4**, 1991 (2013).

[64] A. Misra, U. Singh, S. Bhattacharya, and A. K. Pati, Energy cost of creating quantum coherence, Phys. Rev. A **93**, 052335 (2016).

[65] T. Sagawa and M. Ueda, Minimal energy cost for thermodynamic information processing: Measurement and information erasure, Phys. Rev. Lett. **102**, 250602 (2009).

[66] The Dicke-type interference effect for the single-charger protocol should be distinguished from the collective effect arising from multiple QBs. First, the Dicke-type interference effect can be triggered with only one QB, while the collective effect requires multiple QBs. Second, the strongest collective effect occurs when multiple QBs are concentrated in a very small region or, loosely speaking, at the same location. However, when all superposed positions are identical, the state of the control batteries becomes uncorrelated throughout the entire time period [54], indicating that the quick charging effect does not occur in this scenario.

[67] E. Magesan, J. M. Gambetta, and J. Emerson, Scalable and robust randomized benchmarking of quantum processes, Phys. Rev. Lett. **106**, 180504 (2011).

[68] G. Rubino, L. A. Rozema, A. Feix, M. Araújo, J. M. Zeuner, L. M. Procopio, Č. Brukner, and P. Walther, Experimental verification of an indefinite causal order, Sci. Adv. **3**, e1602589 (2017).

[69] K. Goswami, C. Giarmatzi, M. Kewming, F. Costa, C. Branciard, J. Romero, and A. G. White, Indefinite causal order in a quantum switch, Phys. Rev. Lett. **121**, 090503 (2018).

[70] D. Ebler, S. Salek, and G. Chiribella, Enhanced communication with the assistance of indefinite causal order, Phys. Rev. Lett. **120**, 120502 (2018).

[71] X. Zhao, Y. Yang, and G. Chiribella, Quantum metrology with indefinite causal order, Phys. Rev. Lett. **124**, 190503 (2020).

[72] N. Loizeau and A. Grinbaum, Channel capacity enhancement with indefinite causal order, Phys. Rev. A **101**, 012340 (2020).

[73] G. Chiribella, M. Banik, S. S. Bhattacharya, T. Guha, M. Alimuddin, A. Roy, S. Saha, S. Agrawal, and G. Kar, Indefinite causal order enables perfect quantum communication with zero capacity channels, New J. Phys. **23**, 033039 (2021).

[74] K. Simonov, G. Francica, G. Guarnieri, and M. Paternostro, Work extraction from coherently activated maps via quantum switch, Phys. Rev. A **105**, 032217 (2022).

[75] G. Francica, Causal games of work extraction with indefinite causal order, Phys. Rev. A **106**, 042214 (2022).

[76] H. Nie, T. Feng, S. Longden, and V. Vedral, Quantum cooling activated by coherently-controlled thermalisation, arXiv:2201.06954.

[77] G. Zhu, Y. Chen, Y. Hasegawa, and P. Xue, Charging quantum batteries via indefinite causal order: Theory and experiment, Phys. Rev. Lett. **131**, 240401 (2023).